Ion-Pair Dissociation Dynamics of Cl_2 in the Range 13.26−13.73 eV Studied by Using XUV Laser and the Velocity Map Imaging Method

Yusong Hao, Chang Zhou, and Yuxiang Mo*

Department of Physics and Key Laboratory for Atomic and Molecular Nanosciences, Tsinghua University, Beijing 100084, China

Received: November 6, 2008; Revised Manuscript Received: December 18, 2008

The ion-pair dissociation dynamics of Cl_2 in the range 13.26−13.73 eV have been studied employing coherent extreme ultraviolet radiation (XUV) and the velocity map imaging method. The $Cl^-(^1S_0)$ ion-pair yield spectrum has been measured, and 80 velocity map images of $Cl^-(^1S_0)$ have been recorded for the strong peaks in the spectrum. From the images, two dissociation channels corresponding to $Cl^-(^1S_0) + Cl^+(^3P_j)$ and $Cl^-(^1S_0) + Cl^+(^1D_2)$ have been found. The branching ratios among the fragments $Cl^+(^3P_{0,1})$, $Cl^+(^3P_2)$, and $Cl^+(^1D_2)$ and their corresponding anisotropy parameters β have been determined. It is concluded that the ion-pair dissociation occurs via the predissociation of Rydberg states and its dynamics strongly depend on the excitation energies. The perpendicular and parallel transitions correspond to the excitation to two major Rydberg series converging to ion-core $Cl_2^+(A^2\Pi_u)$,...$\sigma_g^2\pi_u^3\pi_g^4[A^2\Pi_u]ns\sigma_g$, $^1\Pi_u$ ($n = 6,7$), and...$\sigma_g^2\pi_u^3\pi_g^4[A^2\Pi_u]nd\pi_g$, $^1\Sigma_u^+$ ($n = 4,5$), respectively. For the production of fragments $Cl^+(^1D_2)$, it is proposed that the perpendicular transitions are from the excitation to Rydberg states $[A^2\Pi_u]ns\sigma_g$, $^1\Pi_u$ that is predissociated by ion-pair state $2^1\Pi_u$, while the parallel transitions are from the excitation to $[A^2\Pi_u]nd\pi_g$, $^1\Sigma_u^+$ that interacts with ion-pair states $0_u^+(^1D_2)$, $0_u^+(^3P_2)$, and $0_u^+(^3P_0)$.

I. Introduction

The chlorine molecule is one of the benchmark molecules for studying the electronic structures and photochemistry of diatomic molecules. For Cl_2, there are 24 valence electronic states (Λ−S approximation) in which the covalent states and ion-pair states both have 12 states.[1,2] Although there are only two bound covalent states, including the ground electronic states, all ion-pair states are bound states. Therefore, the ion-pair states of Cl_2 are particularly important in characterizing its electronic structure.

The spectroscopic properties of all 12 states (Ω approximation) correlating with $Cl^-(^1S_0) + Cl^+(^3P_j)$ have been studied by using optical−optical double resonance method.[3−7] The fluorescence spectra from the ion-pair state $1^1\Sigma_u^+$ correlating with $Cl^-(^1S_0) + Cl^+(^1D_2)$ have been also observed.[8−10] These spectroscopic studies have provided detailed information about the ion-pair states near their equilibrium bond lengths (∼2.9 Å) that are far from the Franck−Condon region (∼2 Å), and also near their electronic term energies (∼8 eV)[1] that are much lower than the thresholds for ion-pair dissociation (∼11.8 eV for $Cl^-(^1S_0) + Cl^+(^3P_j)$ and ∼13.3 eV for $Cl^-(^1S_0) + Cl^+(^1D_2)$; for comparison, the first adiabatic ionization energy for Cl_2 is ∼11.5 eV).

Berkowitz et al. have studied the ion-pair dissociation dynamics of Cl_2 by measuring the Cl^- ion-pair yield spectrum using extreme ultraviolet (XUV) radiation from both the hydrogen many-line spectrum and the Hopfield continuum of helium with a resolution of 0.14 Å.[11] Their observed spectrum consists of four distinct bands from 105 to 75 nm. The two lowest bands correlate with $Cl^-(^1S_0) + Cl^+(^3P_j)$ in energy. Recently, we have studied the ion-pair dissociation dynamics corresponding to the second lowest band using the velocity map imaging and XUV laser (photon energies: 12.41−12.74 eV).[12] The ion-pair dissociation dynamics was explained by predissociation of Rydberg states converging to ion-core $Cl_2^+(A^2\Pi_u)$. It is found that for most of the predissociations the projection of the total electronic angular momentum (Ω) on the molecular axis is conserved.[12]

Berkowitz et al. inferred that the other two bands in the ion-pair yield spectra have asymptotes of $Cl^-(^1S_0) + Cl^+(^1D_2)$ and $Cl^-(^1S_0) + Cl^+(^1S_0)$, respectively. At the threshold for formation of $Cl^-(^1S_0) + Cl^+(^1D_2)$, they observed an abrupt onset in the ion-pair yield spectrum. From this fact, they suggested that the signals in the spectrum should correlate with the channel of $Cl^-(^1S_0) + Cl^+(^1D_2)$. The observed structure in the ion-pair spectrum was proposed to be from the predissociation of Rydberg series $R^1\Pi_u$, although detailed assignment could not be provided.[11] Two important questions about the dynamics have not yet been answered: (1) are there any Rydberg series other than $R^1\Pi_u$ that correlate with the production of $Cl^-(^1S_0) + Cl^+(^1D_2)$? (2) Is the dissociation $Cl^-(^1S_0) + Cl^+(^1D_2)$ the only channel or even the major channel for photon energies higher than the threshold?

In this paper, we will report our studies on ion-pair dissociation of Cl_2 in the energy range of 13.26−13.73 eV employing XUV laser and velocity map imaging methods. In contrast with the previous conclusions, two dissociation channels, $Cl^-(^1S_0) + Cl^+(^1D_2)$ and $Cl^-(^1S_0) + Cl^+(^3P_j)$, have been found. In addition to this, the relative branching ratios and the angular distributions of photofragments strongly depend on the excitation photon energies.

II. Experimental Section

The details of our XUV photoion spectrometer have been described previously,[12−17] so only a brief summary is given here. The coherent XUV radiation was generated using the resonance enhanced four-wave sum mixing ($2\omega_1 + \omega_2$) in a pulsed Kr jet. An Nd:YAG (YAG-yttrium aluminum garnet) (20 Hz)

* To whom correspondence should be addressed. E-mail: ymo@mail.tsinghua.edu.cn.

10.1021/jp8097878 CCC: $40.75
Published on Web 02/16/2009

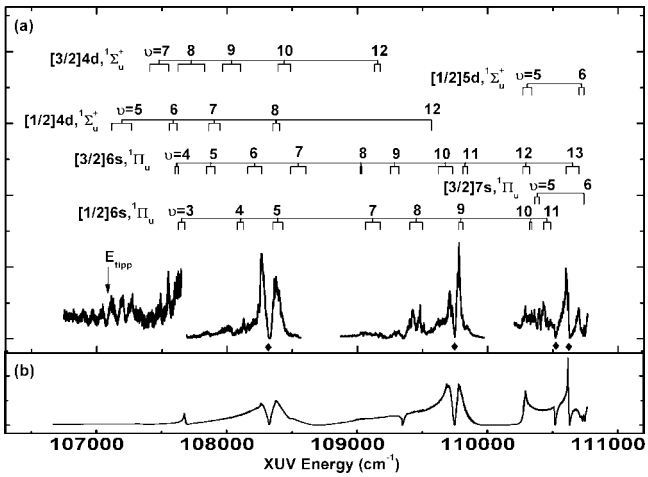

Figure 1. (a) $^{35}Cl^-$ ion-pair yield spectrum: $Cl_2 + h\upsilon \rightarrow {}^{35,37}Cl^+(^3P_j, {}^1D_2) + {}^{35}Cl^-(^1S_0)$ under zero electric field; an extraction field ~580 V/cm was exerted after a delay of ~300 ns relative to the XUV laser pulses. The $^{35}Cl^-$ signal intensities have not been normalized with the XUV light intensities. In the two discontinuous energy regions, the XUV light intensities were so low that reliable $^{35}Cl^-$ signals have not been recorded. There are four signal dips labeled by symbols ◆ resulting from the dips of XUV light intensities. The E_{tipp} indicates the threshold for ion-pair production: $Cl^+(^1D_2) + {}^{35}Cl^-(^1S_0)$. The Rydberg state assignments are also shown. It is noted that the assignments are only for peaks at which $Cl^-(^1S_0)$ velocity map images have been measured. Expanded figures showing the details of the spectrum are shown in Figure 2. (b) XUV light intensities as function of photon energies.

pumped two-dye laser system was used in the experiments. One beam produced by tripling the dye-laser frequency was fixed to match the two-photon resonance ($2\omega_1$) frequency of the $Kr4p^5(^2P_{3/2})5p[1/2]_0 \leftarrow (4p^6)^1S_0$ transition at 94 092.09 cm^{-1}. The other dye laser was tuned from 600 to 770 nm.

In the measurement of the ion-pair yield spectrum, the ion and XUV light signals were fed into two identical boxcars (SR 250, Stanford Research Systems) and transferred to a personal computer. To record the ion-pair yield spectrum under zero electric field, a pulsed electric field was used to extract the $^{35}Cl^-$ fragments after a delay of ~300 ns relative to the XUV laser pulses. The Cl_2 gas sample was premixed with Kr (Kr 94%, Cl_2 6%), and the stagnation pressure was about 1000 torr at room temperature. Since the mass of Kr is comparable to that of Cl_2, the Kr carrier gas should provide better cooling for the Cl_2 beam than other rare gases. The frequencies of the dye lasers were calibrated using He/Ne and He/Ar optogalvanic lamps. Our velocity map imaging method follows that of Parker and co-workers.[18]

III. Results and Discussion

A. Ion-Pair Yield Spectrum and Its Assignments. Panel a of Figure 1 shows the $^{35}Cl^-$ ion-pair yield spectrum of Cl_2 under zero electric field in the range 106 600−110 900 cm^{-1}. Figure 2 is an expanded view of Figure 1 with index numbers on peaks at which we have measured images. The $^{35}Cl^-$ signal intensities have not been normalized with the XUV light intensities since the fluctuations of light intensities at certain photon energies were so large that the normalization was difficult. The spectrum of XUV light intensity shown in panel b of Figure 1 is mainly determined by the efficiency of the nonlinear four-mixing process. There are two sections of photon energies in which the XUV light intensities were so low that the $^{35}Cl^-$ signals could not be obtained. There are also four symbols ◆ in the spectrum, which indicate the dips of the signals due to the very low XUV intensities. The ion-pair yield spectrum with excitation energies ranging from 11.4 to 16.3 eV has been previously reported by Berkowitz et al.[11]

As observed by Berkowitz et al., the ion-pair yield spectrum is characterized by broad background overlapped with some resolved structures. Based on this observation and also the similarity between the ion-pair yield spectrum and photoionization efficiency spectrum (PIE), Berkowitz et al. proposed that the ion-pair dissociation should occur via the predissociation of Rydberg states converging to ion-core...$(\sigma_g3p)^2(\pi_u3p)^3(\pi_g3p)^4$, $Cl_2^+(A^2\Pi_u)$. The ion-pair yield spectrum shown in Figure 2 has higher resolution than the one reported by Berkowitz et al. The well-resolved structures provided stronger supports for a predissociation mechanism of ion-pair dissociation. The broad background may arise from the broadening factors due to the lifetime of the predissociated states, the unresolved rotational structures, the overlapping of different vibrational bands, and also the signals from two different isotopomers, $^{35}Cl_2$ and $^{35}Cl^{37}Cl$, with natural abundance of 9:6.

The probability for excitation to Rydberg states converging to $Cl_2^+(X^2\Pi_g)$ is low in this energy region since it would require very large principal quantum numbers and very high vibrational excitations for the Rydberg series. The Rydberg series converging to ion-core $Cl_2^+(A^2\Pi_u)$ have been observed directly in electron loss spectrum by Stubbs et al.[19] and indirectly in the photoelectron energy spectrum (PES) by Yencha et al.[20] Because of the low resolution of these measurements and the lack of reliable spectroscopic constants for $Cl_2^+(A^2\Pi_u)$, vibrationally resolved assignments for Rydberg states were almost impossible. For a good assignment, accurate vibrational energy levels of $Cl_2^+(A^2\Pi_u)$ are essential.

1. Vibrational Energy Levels for $Cl_2^+(A^2\Pi_u)$. The energy levels of Rydberg series are expressed by the well-known formula

$$E = \mathrm{IE}(A^2\Pi_u, \upsilon^+) - \frac{\mathrm{Ry}}{(n^*)^2} \quad (1)$$

where Ry is the Rydberg constant for Cl_2, n^* is the effective principal quantum number, and $\mathrm{IE}(A^2\Pi_u, \upsilon^+)$ is the ionization energy (IE) for the production of $Cl_2^+(A^2\Pi_u, \upsilon^+)$, which has not yet been determined reliably. However, it can be determined using the relationship

$$\mathrm{IE}(A^2\Pi_u, \upsilon^+) = \mathrm{IE}(X^2\Pi_g, \upsilon') + \Delta E_{\upsilon^+\upsilon'} \quad (2)$$

where $\mathrm{IE}(X^2\Pi_g, \upsilon')$ is the ionization energy for the production of $Cl_2^+(X^2\Pi_g, \upsilon')$, which has been measured recently using zero kinetic energy photoelectron (ZEKE) spectroscopy,[17] and $\Delta E_{\upsilon^+\upsilon'}$ is the energy for the transition $Cl_2^+(A^2\Pi_u, \upsilon^+) \rightarrow Cl_2^+(X^2\Pi_g, \upsilon')$, which can be obtained using the Deslandres tables from the emission spectra of $Cl_2^+(A^2\Pi_u, \upsilon^+) \rightarrow Cl_2^+(X^2\Pi_g, \upsilon')$ measured by Tuckett and Peyerimhoff.[21] The first rows in the Deslandres tables are $\upsilon^+ = 5$ and $\upsilon^+ = 3$ for $Cl_2^+(A^2\Pi_{3/2})$ and $Cl_2^+(A^2\Pi_{1/2})$, respectively, as suggested by Yencha et al.[20,21] The vibrational progressions for υ' are the same as those suggested by Huberman,[22] which have been validated by our previous experimental results.[17]

However, the IE for $Cl_2^+(A^2\Pi_{u,3/2}, \upsilon^+ = 4)$ is from the extrapolation of the experimental data since it has not been observed in the emission spectrum. The vibrational structure for $Cl_2^+(A^2\Pi_u, \upsilon^+)$ is found to be very irregular due to the perturbation by its adjacent electronic states. It is previously noted that the vibrational state of $Cl_2^+(A^2\Pi_{u,3.2})$ can be divided into three groups, in which one group has $\upsilon = 2$, 5, 8, and 11. Based on this observation, we obtained the empirical formula

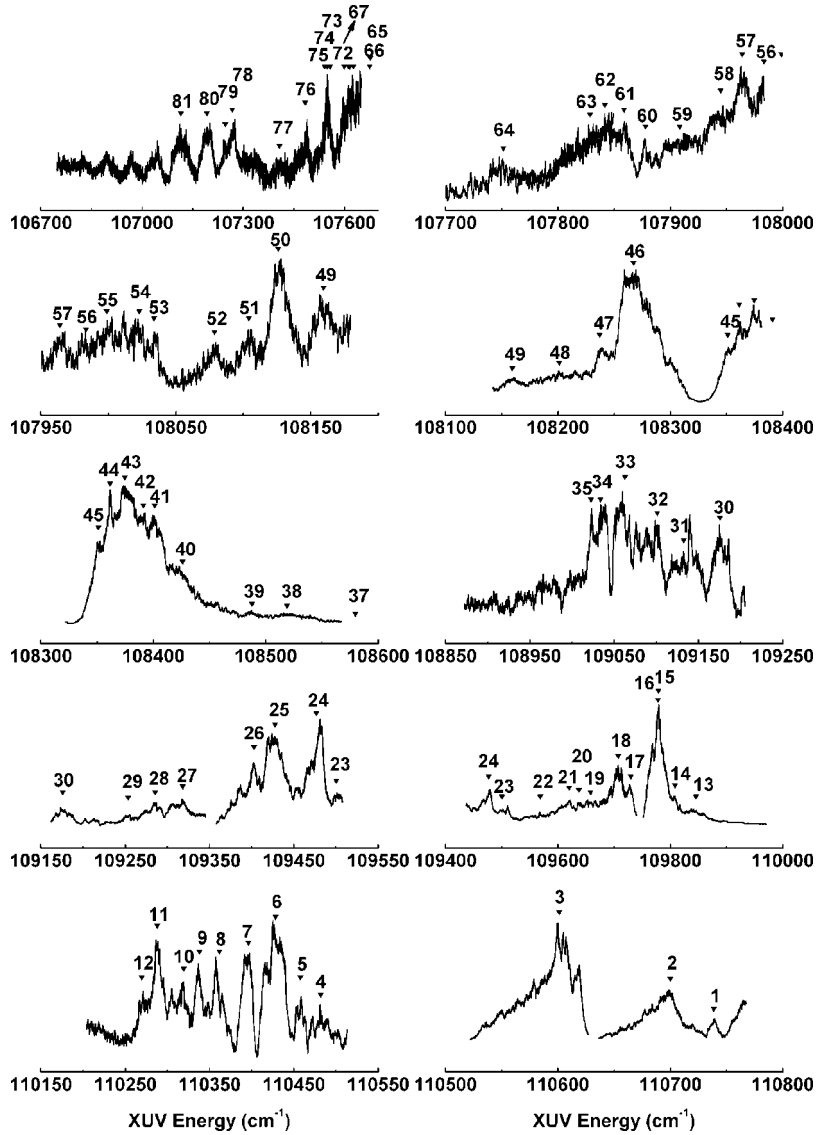

Figure 2. Expanded view for panel a of Figure 1. The symbol ▼ indicates the peak at which an ion image was taken, and the number above it is our index of the image. The energy positions, their assignments, and the related dynamical information can be found in Table 2 by using the index numbers.

for the vibrational energy spacings for this group by applying least-squares fitting to the known experimental data.[21] The result is $\Delta G(v+1) = 320.7 - 2.3\,v$. The accuracy of the extrapolation is estimated to be better than 20 cm^{-1}, which is good enough for quantum defect calculation in our case. The IEs for $Cl_2^+(A^2\Pi_u)$ thus obtained are listed in Table 1.

2. The Assignment of Ion-Pair Yield Spectrum. For halogen molecules, the Rydberg series with low principal quantum numbers should be better described using Hund's case (c). In the studies of Br_2, I_2, and ICl molecules, it is discovered that the strong Rydberg series observed have appreciable singlet character.[23,24] The singlet character in Cl_2 is expected to be stronger than that in Br_2, I_2, and ICl molecules. Therefore, we will use the singlet Rydberg state and $\Lambda-S$ notation in the assignment of the ion-pair yield spectrum. However, it should be remembered that the Rydberg states are not pure singlet states and have some triplet components. The singlet ungerade Rydberg series converging to ion-core $[A^2\Pi_u]$ may have electronic configurations, $[A^2\Pi_u]ns\sigma_g$, $^1\Pi_u(1_u)$, $[A^2\Pi_u]nd\sigma_g$, $^1\Pi_u(1_u)$, $[A^2\Pi_u]nd\pi_g$, $^1\Sigma_u^+(0_u^+)$, $[A^2\Pi_u]nd\delta_g$, $^1\Pi_u(1_u)$, where $[A^2\Pi_u]$ represents the ion-core, and the symbols inside the circular brackets are the notations for Hund's case (c).

As we mentioned, the Rydberg series in this energy region have been observed; in fact, they were assigned only from $[A^2\Pi_u]ns\sigma_g$, $^1\Pi_u$. Stubbs et al. have suggested that the peaks observed in their energy loss spectrum were from three Rydberg series of K, L, and M bands.[19] Based on the more accurate IE determined in their PES, Yencha et al.[20] assigned the L series as Rydberg state $[A^2\Pi_{u,1/2}]5s\sigma_g$, $^1\Pi_u$, and Berkowitz et al.[11] assigned the M band as from $[A^2\Pi_{u,1/2}]6s\sigma_g$, $^1\Pi_u$. All these assignments suggested that the ion-pair dissociation occurs via predissociation of Rydberg states of $^1\Pi_u$ symmetry, which are accessed by perpendicular transitions. As discussed in the following sections, this is in contrast with our experimental findings that both parallel and perpendicular transitions exist. Therefore, another Rydberg series with $^1\Sigma_u^+$ symmetry should exist. The Rydberg series with the required properties has the electron configuration $[A^2\Pi_u]nd\pi_g$, $^1\Sigma_u^+$.

To assign a peak to a particular Rydberg state in the spectrum, we used two criteria. First, the symmetry of the Rydberg state should be in agreement with the observed symmetry from the imaging experiments, e.g., the parallel transition correlating with $[A^2\Pi_u]nd\pi_g$, $^1\Sigma_u^+$, and the perpendicular transition correlating with $[A^2\Pi_u]ns\sigma_g$, $^1\Pi_u$. Second, the effective principal quantum

TABLE 1: Ionization Energy for the Production of $^{35}Cl_2^+(A^2\Pi_u, v)$ Derived by Combining the Data from the ZEKE Spectrum[17] of Cl_2 and the Emission Spectrum[21] of $^{35}Cl_2^+(A^2\Pi_u \rightarrow X^2\Pi_g)$[a]

	$A^2\Pi_{u,3/2}$		$A^2\Pi_{u,1/2}$	
v	$T_0 + G(v)$[b]	IE[c]	$T_0 + G(v)$[b]	IE[c]
3			21 298	114 662
4	21 887*	114 533*	21 658	115 022
5	22 198	114 844	21 983	115 347
6	22 497	115143	22 424	115 788
7	22 944	115 590	22 749	116 113
8	23 250	115 896	23 099	116 463
9	23 551	116 197	23 455	116 819
10	23 966	116 612	23 803	117 167
11	24 263	116 909	24 146	117 510
12	24 564	117 210	24 471	117 835
13	24 945	117 591		
14	25 237	117 883		

[a] The energy unit is in cm^{-1}. [b] T_0 is the electronic term energy of $^{35}Cl_2^+(A^2\Pi_{u,3/2})$ or $^{35}Cl_2^+(A^2\Pi_{u,1/2})$ relative to $^{35}Cl_2^+(X^2\Pi_{g,3/2})$ or $^{35}Cl_2^+(X^2\Pi_{g,1/2})$, respectively. The data in this column is from a combination of ZEKE spectrum and emission spectra. $G(v)$ is the vibrational energy level for v'th vibrational state. [c] The IE represents the ionization energy for the transition $Cl_2^+(A^2\Pi_{u,3/2},v) \leftarrow Cl_2(X^1\Sigma_g^+)$ or $Cl_2^+(A^2\Pi_{u,1/2},v) \leftarrow Cl_2(X^1\Sigma_g^+)$. The IE has an uncertainty of ± 5 cm^{-1}, except the data labeled by *, which is obtained from the extrapolation and has an uncertainty of ~ 20 cm^{-1}.

numbers calculated using eq 1 should be similar to those of the Cl Rydberg atom, which was found to be true previously.[23,24]

The effective principal quantum numbers for 6s Rydberg states of Cl range from 3.86 to 3.93 depending on the states of the ion-core.[25] It is found that the effective principal quantum numbers in the range of 3.93−4.00 for $[A^2\Pi_u]6s\sigma_g$, $^1\Pi_u$ are overall best in assigning the ion-pair yield spectrum. In another respect, the effective principal quantum numbers for Rydberg states $[Cl^+]4d$ and $[Cl^+]5d$ range from 3.55 to 3.80 and from 4.54 to 4.74, respectively.[25] It is found that overall the effective principal quantum numbers in the range of 3.64−3.69 and 4.64−4.69 describe most properly the Rydberg series of $[A^2\Pi_u]4d\pi_g$, $^1\Sigma_u^+$ and $[A^2\Pi_u]5d\pi_g$, $^1\Sigma_u^+$, respectively.

The ion-pair spectrum is not rotationally and vibrationally resolved due to several broadening factors as mentioned in Section III.A. Therefore, two simplifications have been made in the assignment of the spectrum. First, a range of line positions has been assigned from the same vibrational bands with different quantum defects that may be regarded as from different rotational transitions or from two isotopomers. Second, we have assumed that the perpendicular transitions and parallel transitions originated from two Rydberg series $[A^2\Pi_{1/2}]ns\sigma_g$,$^1\Pi_u$ and $[A^2\Pi_u]nd\pi_g$, $^1\Sigma_u^+$, respectively. The possible perpendicular transitions from $[A^2\Pi_u]nd\sigma_g$, $^1\Pi_u$ and $[A^2\Pi_u]nd\delta_g$, $^1\Pi_u$ were not considered, which were assumed previously.[19,20] We also only assigned the peaks that we used in the imaging experiments. Table 2 shows the assignments along with other dynamical parameters discussed below.

For photon energies near the threshold region for the production of $Cl^+(^1D_2)$ (107 096 cm^{-1}), there are some differences between the ion-pair yield spectra under the electric field and under the field free conditions. However, for available energies higher than the Stark shifts $\sim 4\sqrt{E}$ (V/cm), this difference is small due the low principal quantum numbers for Rydberg states in this energy region. In another respect, the electric field usually cannot change the ion-pair dissociation dynamics.[26−28] For example, for electric field of 700 V/cm, the Stark shifts near the threshold are $\sim +4\sqrt{E}$(V/cm), or 0.014 eV. For ion-pair potential at a bond distance of 100 bohr, at which the dissociation is expected to have completed, the Coulomb potential is 0.01 hartree or 0.27 eV, which is much larger than the Stark shifts of 0.014 eV. In this work, we mainly discussed the assignment of the ion-pair yield spectrum and the ion-pair dissociation dynamics about 100 cm^{-1} higher than the threshold for the production of $Cl^+(^1D_2) + Cl^-(^1S_0)$. We have therefore neglected the effect of electric field on the ion-pair yield spectrum and dissociation dynamics.

B. Ion-Pair Dissociation Dynamics.

1. Overview of the Experimental Results. In the 13.27−13.73 eV region, the following two dissociation channels are possible[17]

$$Cl_2 + 107\,096\ cm^{-1} \rightarrow Cl^+(^1D_2) + Cl^-(^1S_0) \quad (3a)$$

$$Cl_2 + 95\,442\ cm^{-1} \rightarrow Cl^+(^3P_{2,1,0}) + Cl^-(^1S_0) \quad (3b)$$

The energy difference between $Cl^+(^1D_2)$ and $Cl^+(^3P_2)$ is 11 654 cm^{-1}, and the energy levels of $Cl^+(^3P_0)$ and $Cl^+(^3P_1)$ relative to $Cl^+(^3P_2)$ are 996 and 696 cm^{-1}, respectively.

Figure 3 shows the $Cl^-(^1S_0)$ images at 80 different photon energies. An index number was given for each image, which was shown at the upper left corner. The inverse Abel transforms were used to obtain the 2-D slices of the 3-D Newton spheres.[12−16] For example, Figure 4 shows an expanded view of four raw images and their inverse Abel transform. Figure 5 shows the angular distributions and center-of-mass (CM) translational energy distributions obtained from the 2-D slice images in Figure 4.

The anisotropy parameters β were obtained by applying the least-squares fitting method to the experimentally obtained angular distributions using the following formula

$$f(\theta) \propto 1 + \beta P_2(\cos\theta) \quad (4)$$

where θ is the angle between the recoil velocity and the polarization direction of the XUV laser and $P_2(x)$ is the second-order Legendre polynomial. In the limiting case of parallel or perpendicular transitions, β equals 2 or -1.[29,30] The relative branching ratios (intensities) for fragments $Cl^+(^1D_2)$and $Cl^+(^3P_j)$ are obtained by integrating the areas of the corresponding peaks in the CM translational energy distributions.

Since the translational energy resolution of our instrument ($\Delta E_{CM}/E_{available}$) was $\sim 5\%$, the fine structures due to $Cl^+(^3P_0)$ and $Cl^+(^3P_1)$ were unable to be resolved in our imaging experiments. In the following discussion, we designate the two components together as $Cl^+(^3P_{0,1})$. For photon energies above 108 000 cm^{-1}, all three spin−orbit components $Cl^+(^3P_{0,1,2})$ were also difficult to be resolved and are designated together as $Cl^+(^3P_j)$. To obtain the branching ratios between $Cl^+(^3P_{0,1})$ and $Cl^+(^3P_2)$, the deconvolution method using Gaussian distribution functions has been applied to the translational energy distributions. To obtain the angular distributions for $Cl^+(^3P_{0,1})$ and $Cl^+(^3P_2)$, we integrated the signals inside the half-heights of their peaks or narrower than these. For some images, we obtained the resolved branching ratios between $Cl^+(^3P_{0,1})$ and $Cl^+(^3P_2)$, but not the corresponding resolved β parameters. The applied photon energies, the β parameters, and the branching ratios among different channels can be found in Table 2 using the index numbers.

Panels a, b, c, and d of Figure 6 show the β values for the production of $Cl^+(^3P_{0,1})$, $Cl^+(^3P_2)$, $Cl^+(^3P_j)$, and $Cl^+(^1D_2)$, respectively. To illustrate the changes of β with the excitation photon energies, panel e of Figure 6 shows the ion-pair yield spectrum. Panels a and b of Figure 7 show the relative branching

TABLE 2: Summary of Experimental Results for Ion-Pair Dissociation: $Cl_2 + h\nu \rightarrow Cl^+(^1D_2, ^3P_j) + Cl^-(^1S_0)$

		relative ratio[c]		β[d]			$[A^2\Pi_{u,3/2}]$[e]			$[A^2\Pi_{u,1/2}]$[e]		
no.[a]	XUV energy[b] (cm^{-1})	$Cl^+(^3P_{0,1})$	$Cl^+(^3P_2)$	$Cl^+(^1D_2)$	$Cl^+(^3P_{0,1})$	$Cl^+(^3P_2)$	*Nl*	*n**	*v*	*nl*	*n**	*v*
1	110 738.8		0.11	−0.62		0.10	7s	4.99	6	5d	4.66	6
2	110 700.0		0.09	−0.78		−0.32	6s	3.99	13	5d	4.64	6
3	110 601.2		0.12	−0.85		−0.64	6s	3.96	13			
4	110 481.9		0.67	−0.92		−0.74				6s	3.95	11
5	110 457.8	0.19	0.16	−0.74		−0.26				6s	3.94	11
6	110 428.3	0.06	0.15	−0.73		0.94				6s	3.94	11
7	110 396.3		0.13	−0.71		−0.53	7s	4.97	5			
8	110 361.8	0.12	0.19	−0.81		−0.61	7s	4.95	5			
9	110 338.0		0.30	−0.94		0.40				6s(5d)	3.99(4.68)	10(5)
10	110 319.5		0.18	−0.68		−0.72	6s	3.99	12	6s	3.99	10
11	110 287.9	0.08	0.12	−0.72		0.95	6s	3.99	12	5d	4.66	5
12	110 269.5		0.17	−0.69		1.05	6s	3.98	12	5d	4.65	5
13	109 845.6		0.63	−1.00		−0.04	6s	3.94	11			
14	109 808.5	0.07	0.53	−1.00		−0.53	6s	3.93	11	6s	3.96	9
15	109 778.8		0.75	−1.00		−1.00				6s	3.95	9
16	109 777.8		0.63	−1.00		−1.00				6s	3.94	9
17	109 729.7	0.50	0.63	−1.00		−0.81	6s	3.99	10			
18	109 707.7	0.12	0.26	−1.00		−0.20	6s	3.99	10			
19	109 657.8	0.23	0.94	−1.00		−0.56	6s	3.97	10			
20	109 637.2		2.14	−0.92		−0.57	6s	3.97	10			
21	109 620.3		1.73	−1.00		−0.95	6s	3.96	10			
22	109 568.5		0.64	−0.80		0.16				4d	3.64	12
23	109 500.4		0.26	−0.93		−0.44				6s	3.97	8
24	109 476.7		0.39	−0.96		−0.85				6s	3.96	8
25	109 427.7		0.22	−0.81		−0.05				6s	3.95	8
26	109 402.9		0.45	−0.96		−0.30				6s	3.94	8
27	109 318.0		1.07	−0.86		−0.88	6s	3.99	9			
28	109 285.7		0.78	−0.84		−0.68	6s	3.98	9			
29	109 253.4		0.56	−0.93		−0.59	6s	3.98	9			
30	109 175.7	0.19	0.12	−0.90	1.92	0.28	4d	3.70	12	6s	3.98	7
31	109 132.6	0.12	0.18	−0.76	0.74	0.24	4d	3.69	12	6s	3.97	7
32	109 101.0		0.72	−0.82		−0.90				6s	3.96	7
33	109 062.8		3.09	−0.79		−0.85				6s	3.95	7
34	109 033.8		5.28	−1.00		−1.00	6s	4.00	8			
35	109 022.6		8.31	−0.37		−0.91	6s	4.00	8			
36	108 605.0		2.96	−0.97		−0.85	6s	3.96	7			
37	108 579.7		2.18	−1.00		−0.88	6s	3.96	7			
38	108 519.0		0.93	−0.89		−0.64	6s	3.94	7			
39	108 487.9		2.59	−0.66		0.34	6s(4d)	3.93(3.68)	7(10)			
40	108 425.9	0.53	0.95	−0.52		1.24	4d	3.66	10	6s	3.98	5
41	108 401.2	0.27	0.48	−0.82		0.86	4d	3.66	10	6s(4d)	3.98(3.69)	5(8)
42	108 391.0	0.53	0.70	−0.83		0.11	4d	3.65	10	6s(4d)	3.97(3.69)	5(8)
43	108 374.6	1.53	1.25	−0.69		−0.43				6s	3.97	5
44	108 361.4	0.33	0.55	−0.67		0.22				6s(4d)	3.96(3.68)	5(8)
45	108 351.0		0.95	−0.85		−0.03				6s(4d)	3.96(3.68)	5(8)
46	108 267.2		3.15	−0.65		−0.57	6s	3.99	6			
47	108 237.1	0.75	1.30	−0.30		−0.14	6s	3.99	6			
48	108 201.2	1.10	1.56	−0.15		0.28	6s	3.98	6			
49	108 159.4		2.67	−0.71		−0.26	6s	3.96	6			
50	108 125.9		3.66	−0.27		−0.11				6s	3.99	4
51	108 104.2	0.30	0.62	−0.70		1.34	4d	3.68	9	6s	3.98	4
52	108 078.7	0.50	0.66	−0.61		1.34	4d	3.68	9	6s	3.98	4
53	108 033.8	0.46	0.48	−0.26	1.98	1.54	4d	3.67	9			
54	108 022.9	0.36	0.38	−0.42	2.00	1.92	4d	3.66	9			
55	107 998.8	0.18	0.16	−0.73	2.00	2.00	4d	3.66	9			
56	107 983.4	0.11	0.14	−0.65		0.64	4d	3.66	9			
57	107 964.1	0.61	0.70	−0.55	2.00	0.65	4d	3.65	9			
58	107 944.8	2.79	2.81	0.38	1.03	0.28				4d	3.67	7
59	107 908.4	1.83	3.84	0.87		−0.19	6s	3.98	5	4d	3.66	7
60	107 877.9	1.25	2.70	1.46	0.67	0.20				4d	3.65	7
61	107 858.9	3.35	4.09	−0.70	0.40	−0.37	6s	3.96	5	4d	3.65	7
62	107 841.8	0.32	1.03	−0.78		−0.10	6s	3.96	5			
63	107 828.6	0.41	0.70	−0.21	2.00	1.37	4d	3.69	8			
64	107 751.5	0.56	0.94	1.22	1.99	0.07	4d	3.67	8			
65	107 676.7	1.29	1.53	−0.71	2.00	1.96	4d	3.65	8	6s	3.96	3
66	107 675.4	0.84	1.37	−0.62	2.00	2.00	4d	3.65	8	6s	3.96	3
67	107 627.2	0.47	0.95	−0.31	2.00	0.91	6s(4d)	3.99(3.64)	4(8)	6s	3.95	3
68	107 623.0	0.50	0.86	−0.58	2.00	1.78	6s(4d)	3.99(3.64)	4(8)			
69	107 616.2	1.26	1.32	−0.30	2.00	1.83	6s	3.98	4	4d	3.66	6

TABLE 2: Continued

		relative ratio[c]		β[d]			$[A^2\Pi_{u,3/2}]$[e]			$[A^2\Pi_{u,1/2}]$[e]		
no.[a]	XUV energy[b] (cm^{-1})	$Cl^+(^3P_{0,1})$	$Cl^+(^3P_2)$	$Cl^+(^1D_2)$	$Cl^+(^3P_{0,1})$	$Cl^+(^3P_2)$	*Nl*	*n**	*v*	*nl*	*n**	*v*
70	107 612.6	0.93	0.92	−0.49	1.95	1.56	6s	3.98	4	4d	3.66	6
71	107 611.6	0.79	0.69	−0.48	1.96	1.72	6s	3.98	4	4d	3.66	6
72	107 599.8	0.51	0.49	−0.47	1.45	0.91	6s	3.98	4	4d	3.66	6
73	107 558.0	0.71	0.72	0.91	2.00	2.00				4d	3.65	6
74	107 549.0	0.97	0.87	1.26	2.00	2.00	4d	3.69	7			
75	107 541.8	0.98	0.94	1.46	2.00	1.96	4d	3.69	7			
76	107 484.3	1.03	1.49	1.54	2.00	1.36	4d	3.68	7			
77	107 407.7	1.21	1.11	0.34	2.00	2.00	4d	3.66	7			
78	107 267.7	2.51	2.05	0.04	2.00	2.00				4d	3.69	5
79	107 246.9	2.73	1.87	−0.36	2.00	2.00				4d	3.68	5
80	107 191.9	9.56	9.08	1.29	2.00	2.00				4d	3.67	5
81[f]	107 115.2									4d	3.65	5

[a] The number sequentially indexes the photon energies used in the measurements. [b] The photon energy in cm^{-1} with uncertainty of ± 1 cm^{-1}. [c] The intensities of $Cl^+(^3P_2)$ and $Cl^+(^3P_{0,1})$ relative to $Cl^+(^1D_2)$, which is assumed to be 1. The uncertainty is ± 0.1. If there is no value listed for $Cl^+(^3P_{0,1})$, the value at column $Cl^+(^3P_2)$ then represents the total intensity for $Cl^+(^3P_2)$ and $Cl^+(^3P_{0,1})$. [d] The anisotropy parameter. The uncertainties are ± 0.05 and ± 0.10 for $Cl^+(^1P_2)$ and $Cl^+(^3P_j)$, respectively. If there is no value listed for $Cl^+(^3P_{0,1})$, the value at column $Cl^+(^3P_2)$ then represents the β for fragments $Cl^+(^3P_2)$ and $Cl^+(^3P_{0,1})$ together. When the relative intensities of $Cl^+(^3P_2)$ or $Cl^+(^3P_{0,1})$ are smaller than 0.1, the uncertainties are ± 0.20. [e] The $[A^2\Pi_{u,3/2}]$ and $[A^2\Pi_{u,1/2}]$ represent Rydberg series with ion core $Cl_2^+(A^2\Pi_{u,3/2})$ and $Cl_2^+(A^2\Pi_{u,1/2})$, respectively. The *n*s and *n*d represent Rydberg states $[A^2\Pi_u]ns\sigma_g$, $^1\Pi_u$ and $[A^2\Pi_u]nd\pi_g$, $^1\Sigma_u^+$, respectively. The *n** and *v* represent the effective principal quantum numbers and the vibrational quantum numbers for the ion-core, respectively. [f] The image at the zero-field is published previously.[22]

ratios among fragments $Cl^+(^3P_2)$ and $Cl^+(^3P_{1,0})$ to $Cl^+(^1D_2)$, respectively. The intensity for $Cl^+(^1D_2)$ is assumed to be unit for each photon energy. Panel c of Figure 7 is the ion-pair yield spectrum showing the band positions for the measured branching ratios.

An examination of Figures 6 and 7 shows that the β parameters and the branching ratios among fragments $Cl^+(^1D_2)$ and $Cl^+(^3P_j)$ depend strongly on the excitation photon energies. In the 107 115−107 964 cm^{-1} region, the major channels are the production of $Cl^+(^3P_j)$, and most of them are from parallel transitions with β nearly the limiting value of +2, while the channels for the production of $Cl^+(^1D_2)$ have both positive and negative β values. In the 107 964−110 740 cm^{-1} region, the β values for the $Cl^+(^1D_2)$ channels are all negative, and most of the β values for the $Cl^+(^3P_j)$ channels are also negative; however, some of them have positive values. In the 109 100−110 740 cm^{-1} region, the major channels are the production of $Cl^+(^1D_2)$.

The ion-pair dissociation of Cl_2 was explained by the predissociation mechanism.[11,12] The couplings between the ion-pair states and Rydberg states may arise from two kinds of interaction: homogeneous and heterogeneous.[31] The heterogeneous interaction involves the coupling of the nuclear rotational motion with the electronic motion or the so-called Coriolis interaction. In our experimental conditions,[17] the rotational temperature of the parent molecule was ∼10 K, and hence it is expected that ion-pair dissociation occurs mainly via the homogeneous perturbation ($\Delta\Omega = 0$) between Rydberg states and ion-pair states. As we will show in next section, this homogeneous perturbation originates from the electrostatic perturbation.

2. Diabatic Potential Energy Curves (PECs) and Adiabatic State Correlation Diagram. For Cl_2, the PECs of ion-pair states correlating with the channels of eqs 3a and 3b have been calculated in both Λ−S (without spin−orbit coupling) and Ω (with spin−orbit coupling) approximations by Kokh et al.[1,2] In these calculations, the interactions of ion-pair states with low Rydberg states converging to $Cl_2^+(X^2\Pi_g)$ have been taken into account. All PECs show the typical double minimum structures due to the avoided crossing between Rydberg states and ion-pair states with the same symmetries. However, the adiabatic PECs considering the interaction of ion-pair states with Rydberg states converging to $Cl_2^+(A^2\Pi_u)$ have not yet been reported.

To understand the dynamics, we calculated the diabatic PECs of the ion-pair states at the level of multireference internally contracted configuration interaction (MRCI) using the MOLPRO software package.[32] The reference functions for MRCI are from complete active space-SCF (CASSCF) calculation employing the contracted aug-cc-pVTZ basis sets. The calculations used the D_{2h} instead of the $D_{\infty h}$ symmetry group for the sake of technical simplicity.[32] The diabatic means that the electronic configurations involving the Rydberg electron had not been included in the calculation. Figure 8 shows such PECs with ungerade symmetry. The vibrational wave function of the $v = 0$ level of the neutral ground $Cl_2(X^1\Sigma_g^+)$ is also displayed in Figure 8 to show the Franck−Condon region where the vertical excitations occur most easily. A comprehensive and accurate calculation of adiabatic PESs can be found in works by Kokh et al.[1,2]

The calculation of PEC for Rydberg states converging to $Cl_2^+(A^2\Pi_u)$ is difficult. However, the PEC for the Rydberg state should be similar to that of the converged cation if the coupling between Rydberg state and ion-pair state is neglected. The PEC of Rydberg state $[A^2\Pi_u]6s\sigma_g$, $^1\Pi_u$, as shown in Figure 8, is obtained by shifting that of the $Cl_2^+(A^2\Pi_u)$ to the experimentally determined energy position of $[A^2\Pi_u]6s\sigma_g$, $^1\Pi_u$. The PEC of $Cl_2^+(A^2\Pi_u)$ was calculated at the level of MRCI/CAS/avtz using MOLPRO software.[32] The PECs including the spin−orbit interaction would provide deeper insights into the interaction among the ion-pair states. Figure 9 shows the correlation diagram based on such kind of calculation by Kokh et al.[2] The avoided crossings due to the same symmetries are indicated as dots in the figure.

The main electronic configurations of ion-pair states at the Franck−Condon region are also shown in Figure 9. For ion-pair states $1^1\Sigma_u^+$, $1^3\Sigma_u^-$, $2^3\Pi_u$, and $2^1\Pi_u$, their electronic configurations differ by two with those of Rydberg series converging to ion-core $Cl_2^+(A^2\Pi_u)$. This means that the predissociation between the ion-pair states and the Rydberg series could occur via electrostatic perturbation ($1/r_{ij}$).[31] In another respect, the spin−orbit interaction usually requires that the two interacting states should differ by only one orbital.[31] This indicates that the probability of predissociation due to the spin−orbit perturbation between the ion-pair states and the Rydberg series converging $Cl_2^+(A^2\Pi_u)$ is rare.

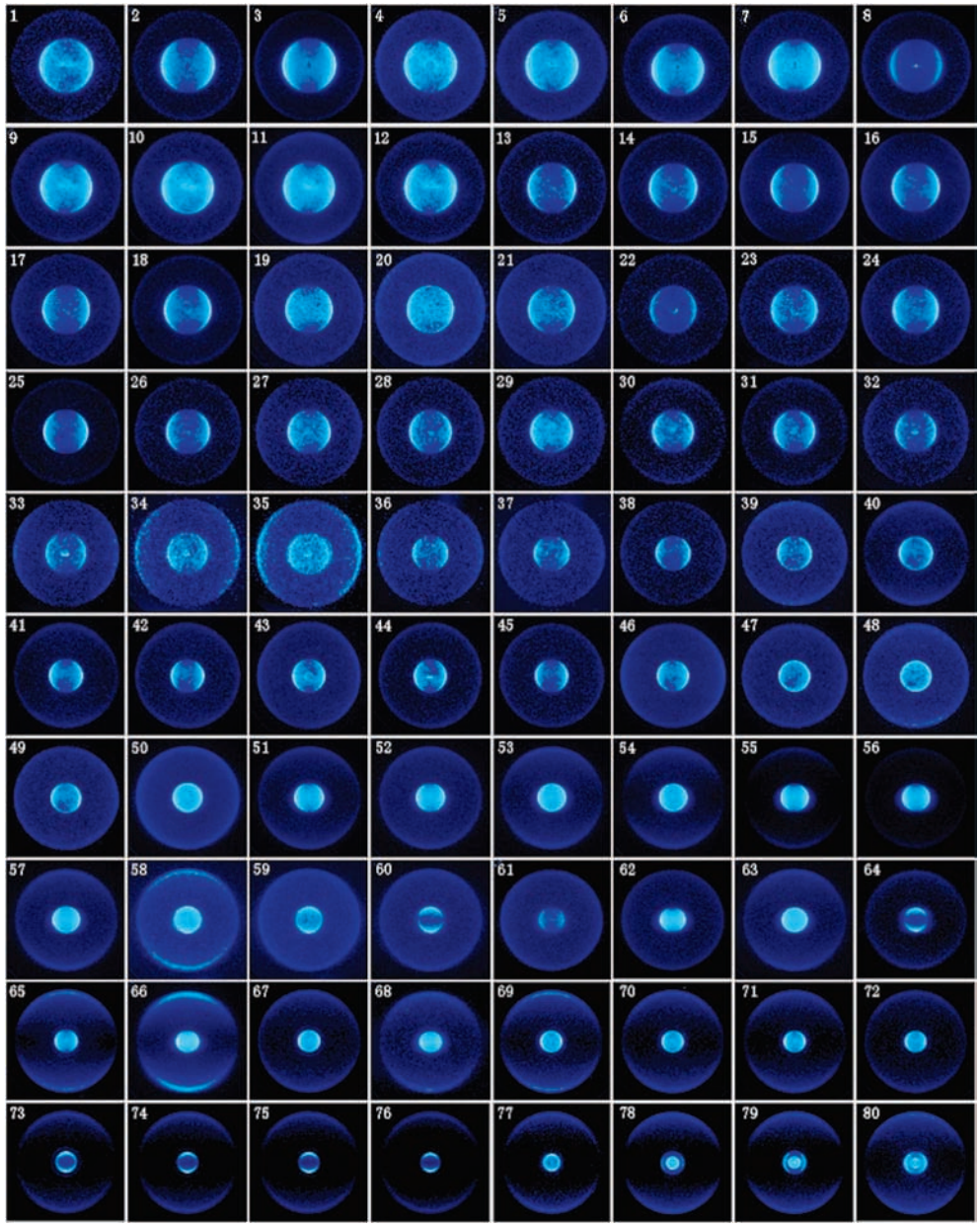

Figure 3. Velocity map imagings of Cl^- from the ion-pair dissociation of Cl_2. Each image has an index number at the upper left corner. The applied photon energies, the anisotropy parameters β, and the branching ratios among different dissociation channels can be found in Table 2 using the index numbers. The polarization of XUV laser is in the imaging plane and along the up-and-down direction. Please note that the brightness and contrast for each image have been adjusted to show clearly the two components $Cl^+(^3P_j)$ and $Cl^+(^1D_2)$. The extraction field strengths were ~430 V/cm for images $N = 65$, 67, and 69−81, and all others were ~580 V/cm.

In the adiabatic picture, the PECs correlating with the ion-pair states asymptotically will have the Rydberg electronic configuration in the Franck−Condon region due to the avoided crossing. For example, the electronic configuration for the inner well of $2^1\Pi_u$ is Rydberg state $[X^2\Pi_g]$, $4p\sigma_u$.[1] On the other hand, the PEC with the ion-pair electronic configuration $\sigma_g^1\pi_u^3\pi_g^4\sigma_u^2$ in the Franck−Condon region will correlate with the production of Cl Rydberg state asymptotically.[1] Therefore, it is very difficult to find states lying in the ionization energy region which maintain the electron configurations of ion-pair states from the Franck−Condon region to the asymptotes. This suggests that the ion-pair dissociation should usually occur via predissociation process or coupling of Rydberg states with ion-pair states, which is supported by most of the reported experimental results. In the diabatic picture used in the following discussion, the predissociation occurs via the electrostatic perturbation between Rydberg states and ion-pair states.

For excitation energies in the 13.26−13.73 eV region, it is seen from Figure 8 that the repulsive parts of the ion-pair state $1^3\Sigma_u^-$ and $2^3\Pi_u$ are accessible to the vertical excitation. However, the transition dipole moments for them are very small since their electronic orbitals differ by two with those of the ground state of Cl_2 in the Franck−Condon region. In contrast to this, the excitation to $1^1\Sigma_u^+$ has a large transition dipole moment, and it has already been observed in spectroscopic studies.[8−10,33] However, for photon energies ~13.3 eV, the vertical excitation is out of the Franck−Condon region. Hence, the direct ion-pair dissociation via $1^1\Sigma_u^+$ is difficult.

3. Dynamics for Singlet Channel $Cl^+(^1D_2)$. It is seen from Figure 9 that there are three singlet ion-pair states $1^1\Delta_u$, $1^1\Sigma_u^+$, and $2^1\Pi_u$ (Λ−S approximation) correlating with the channel for the production of $Cl^+(^1D_2)$. Direct excitation to ion-pair states can occur only for ion-pair state $1^1\Sigma_u^+$, which is difficult due to the unfavorable Franck−Condon factors in this energy region.

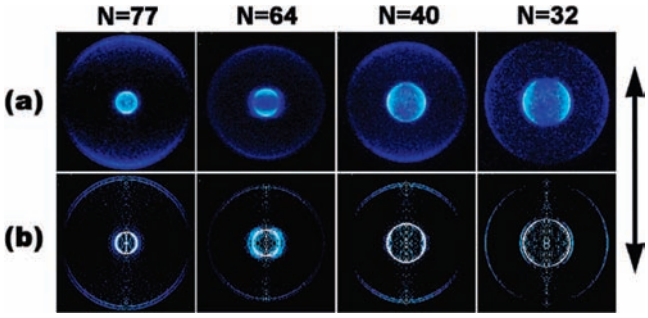

Figure 4. Four images of Cl^- from the ion-pair dissociation of Cl_2. Panel a shows the raw experimental images, and panel b shows the 2-D slice images from the inverse Abel transform of the raw images. The polarization of the XUV laser is indicated in the figure. The numbers above the images are our index numbers. The center-of-mass translational energy distributions and angular distributions of the photofragments obtained from these images are shown in Figure 5. The extraction field strengths are ~430 V/cm for image $N = 77$ and 580 V/cm for the other three images. The brightness and contrast for each image have been adjusted to show clearly the two components $Cl^+(^3P_j)$ and $Cl^+(^1D_2)$.

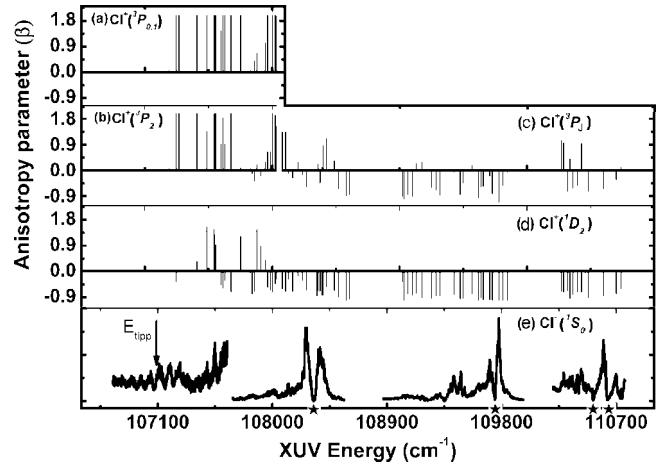

Figure 6. Partially spin−orbit state resolved anisotropy parameters β. Panels a, b, c, and d are for $Cl^+(^3P_{0,1})$, $Cl^+(^3P_2)$, $Cl^+(^3P_j)$, and $Cl^+(^1D_2)$, respectively. Panel e is the ion-pair yield spectrum showing the energy positions of the measured anisotropy parameters.

However, the ion-pair dissociation may occur via predissociation of Rydberg states. Since one-photon excitation can only prepare Rydberg states of $\Omega = 0$ and 1, predissociation may occur for ion-pair states $1^1\Sigma_u^+$ and $2^1\Pi_u$ via homogeneous perturbation. The predissociation of $[A^2\Pi_u]6s\sigma_g$ by $2^1\Pi_u$ is expected to occur easily since there is a crossing point between them near the Franck−Condon region as seen in Figure 8. This suggests that the overlap integral between the vibrational function of $[A^2\Pi_u]6s\sigma_g$ and the nuclear scattering wave function of $2^1\Pi_u$ is favorable, which supports a strong coupling between them. It is hence concluded that the fragment $Cl^+(^1D_2)$ should be mainly originated from the predissociation of $[A^2\Pi_u]ns\sigma_g$, $^1\Pi_u$ by ion-pair state $2^1\Pi_u$, which results in perpendicular transitions. This is just what we observed in experiments for excitation energies higher than 107 964 cm^{-1}.

However, as can be seen from Table 2, parallel transitions for $Cl^+(^1D_2)$ do exist for lower excitation energies. This may arise from a parallel transition to Rydberg series $[A^2\Pi_u]nd\pi_g$, $^1\Sigma_u^+$ predissociated by state $0_u^+(^1D_2)$. The main component of $0_u^+(^1D_2)$ is the $\Omega = 0$ component of $2^3\Pi_u$ in the Franck−Condon region and is the ion-pair state $1^1\Sigma_u^+$ in the post-Franck−Condon region. Since the interaction between $2^3\Pi_u$ and $[A^2\Pi_u]nd\pi_g$, $^1\Sigma_u^+$ is weak, it is thus expected that the probability for the production of $Cl^+(^1D_2)$ via parallel transition is low, which is supported by the experimental results. In fact, there is a state mixing among $0_u^+(^1D_2)$, $0_u^+(^3P_0)$, and $0_u^+(^3P_2)$ due to spin−orbit interaction. Therefore, the parallel transitions for $Cl^+(^1D_2)$ may arise from the excitation to Rydberg states $[A^2\Pi_u]nd\pi_g$, $^1\Sigma_u^+$ and its interaction with ion-pair states $0_u^+(^1D_2)$, $0_u^+(^3P_0)$, and $0_u^+(^3P_2)$. This suggests that if the channel of $Cl^+(^1D_2)$ is from parallel transition at certain photon energy, the $Cl^+(^3P_0)$ and $Cl^+(^3P_2)$ should be also in parallel transition. As shown in Table 2, when β for $Cl^+(^1D_2)$ is positive, the β for $Cl^+(^3P_j)$ is also positive except the data for image $N = 59$.

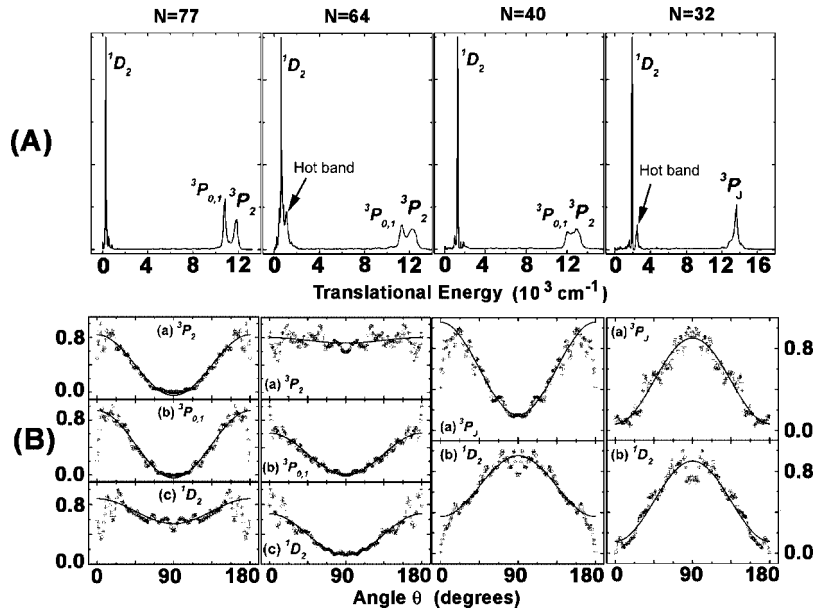

Figure 5. (a) Center-of-mass translational energy distributions for ion-pair dissociation and (b) the partially spin−orbit state resolved angular distributions for ion-pair dissociation. The numbers above the images are our index numbers. For angular distributions, the dots in the figures are the data obtained from the 2-D slices of the Abel transform. The solid curves are the least-squares fittings using eq 4. The fluctuations of the data near 0° and 180° are from noises inherent to Abel transform, which have not been used in the least-squares fittings.

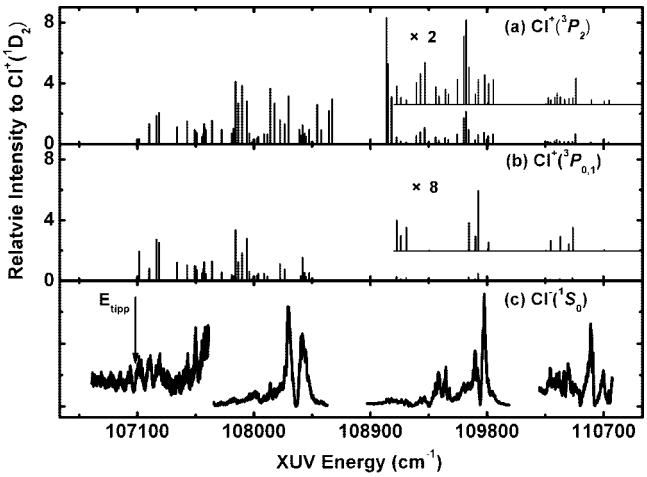

Figure 7. Branching ratios among $Cl^+(^3P_{0,1})$, $Cl^+(^3P_2)$, and $Cl^+(^1D_2)$. The intensity for $Cl^+(^1D_2)$ is assumed to be unit for each photon energy. Panels a and b are intensities of $Cl^+(^3P_2)$ and $Cl^+(^3P_{0,1})$, respectively. However, when the data for $Cl^+(^3P_{0,1})$ are not shown, the data for $Cl^+(^3P_2)$ represent the total intensities of $Cl^+(^3P_2)$ and $Cl^+(^3P_{0,1})$; see Table 2 for details. Panel c is the ion-pair yield spectrum showing the relative energy positions of the measured branching ratios.

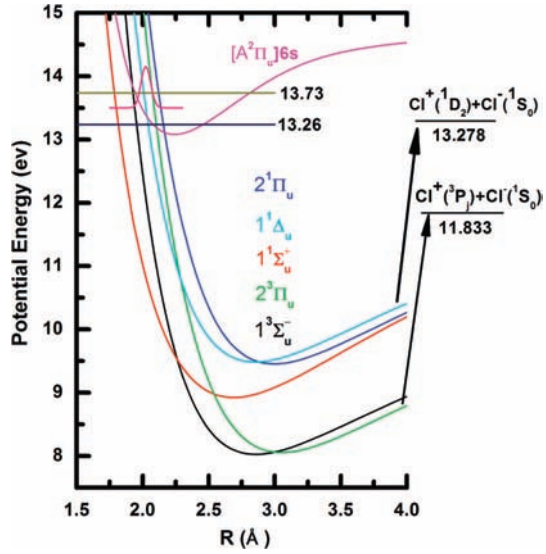

Figure 8. Diabatic ion-pair potential energy curves of Cl_2 calculated at the level of MRCI/CAS/avtz. The diabatic means that the electronic configurations involving the Rydberg electron had not been included in the calculation. The potential energy curve of Rydberg state $[A^2\Pi_u]6s\sigma_g$ was obtained by shifting that of the $Cl_2^+(A^2\Pi_u)$ to the experimentally determined energy position. The vibrational wave function of the $v = 0$ level of the neutral ground $Cl_2(X^1\Sigma_g^+)$ is also displayed in Figure 8 to indicate the Franck−Condon region.

4. Dynamics for Triplet Channel $Cl^+(^3P_j)$. In Λ−S approximation, the channels for the production of $Cl^+(^3P_j)$ correlate with triplet ion-pair state $^3\Sigma_u^-$ and $^3\Pi_u$. Since the predissociated Rydberg states consist mainly of single state components, the ion-pair states should be better described using Hund's case (c) coupling scheme in which S is not a good quantum number.

From Figure 9, it is seen that the fragments $Cl^+(^3P_0)$ correlate only with ion-pair state $0_u^+(^3P_0)$ that gives rise to parallel transitions. The fragment $Cl^+(^3P_1)$ correlates with the ion-pair states $1_u(^3P_1)$ and $0_u^-(^3P_1)$. The latter is unable to have homogeneous interaction with Rydberg states prepared by one-photon excitation. If the heterogeneous interaction is weak, it is expected that the fragments $Cl^+(^3P_0)$ should be mainly produced in parallel transitions and the fragments $Cl^+(^3P_1)$ should be mainly

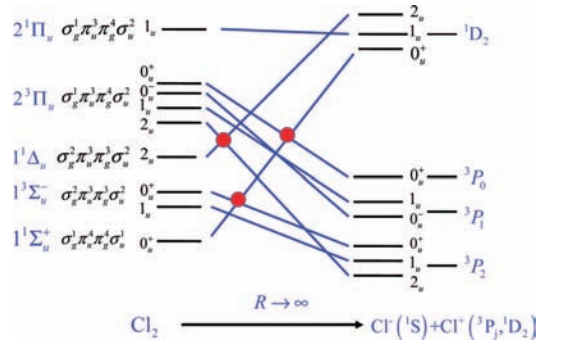

Figure 9. Adiabatic state correlation diagram for ion-pair dissociation of Cl_2 based on the multiconfiguration *ab initio* calculations including spin−orbit perturbation by Bunker et al.[1,2] The small dots in the diagram indicate the avoided crossings due to the adiabatic interactions among 0_u^+ or 2_u states.

produced in perpendicular transitions. This phenomenon has been observed in our studies of Cl_2 in the photon energy region 12.41−12.74 eV.[12] Unfortunately, in this study, the resolution is not good enough to distinguish fragment $Cl^+(^3P_0)$ from $Cl^+(^3P_1)$. It is seen that the β values for the unresolved fragments $Cl^+(^3P_{0,1})$ are all positive for excitation energies lower than 107 964 cm^{-1} (see panels a, b, and c of Figure 6). This means that the cross sections for the production of $Cl^+(^3P_0)$ are larger than those of $Cl^+(^3P_1)$.

The channel for the production of $Cl^+(^3P_2)$ correlates with ion-pair states $0_u^+(^3P_2)$ and $1_u(^3P_2)$, which are mainly the $\Omega = 0_u^+$ and $\Omega = 1_u$ components of the state $1^3\Sigma_u^-$ in the Franck−Condon region, respectively. The states $0_u^+(^3P_2)$ and $1_u(^3P_2)$ can interact with Rydberg series $[A^2\Pi_u]nd\pi_g$, $^1\Sigma_u^+(0_u^+)$ and $[A^2\Pi_u]$-$ns\sigma_g$, $^1\Pi_u(1_u)$, respectively, which result in parallel and perpendicular transitions, respectively.

5. Examples: Dynamics at Four Photon Energies. From the above discussions, it is known that for Cl_2 in one-photon excitation two major Rydberg series are excited: $[A^2\Pi_u]nd\pi_g$ with symmetry $^1\Sigma_u^+$ or 0_u^+ and $[A^2\Pi_u]ns\sigma_g$ with symmetry $^1\Pi_u$ or 1_u, which lead to parallel and perpendicular transitions, respectively. It is expected that the ion-pair dissociation dynamics vary with the excitation photon energies since different Rydberg series may appear alternatively with photon energies, which is illustrated by Figure 6. In the following, we will explain qualitatively the main characteristics of the ion-pair dissociation dynamics at four excitation energies corresponding to our index numbers, $N = 77$, 64, 40, and 32 in Table 2. Their images are shown in Figure 4. The corresponding angular distributions and CM translational energy distributions are shown in Figure 5.

(i) For $h\nu = 107\,407.7$ cm^{-1} ($N = 77$), this peak is assigned as $[A^2\Pi_{u,3/2}]4d\pi_g$, $^1\Sigma_u^+$ with $v = 7$ and $n^* = 3.66$. The β for channels $Cl^+(^3P_{0,1})$, $Cl^+(^3P_2)$, and $Cl^+(^1D_2)$ are 2.0, 2.0, and 0.34, and the branching ratios for them, which were obtained by integrating the areas of the corresponding peaks, are 1.21, 1.11, and 1, respectively (the intensity for $Cl^+(^1D_2)$ is always assumed to be 1, as mentioned). The β value for the production of $Cl^+(^1D_2)$ is smaller than 0.5; it suggests that in addition to the parallel transition, a large percent of $Cl^+(^1D_2)$ comes from perpendicular transition. A possible candidate of Rydberg state for the perpendicular transition is $[A^2\Pi_{u,3/2}]4d\sigma_g$, $^1\Pi_u$ which is neglected in the above discussions. The nonadiabatic interaction among ion-pair states $0_u^+(^3P_0)$, $0_u^+(^3P_2)$, and $0_u^+(^1D_2)$ may occur for the production of $Cl^+(^1D_2)$. In another respect, fragment $Cl^+(^3P_1)$ should be usually from perpendicular transition. The limiting value of $\beta = 2$ for fragments $Cl^+(^3P_{0,1})$ suggests that the intensity for $Cl^+(^3P_1)$ may be weak.

(ii) For $h\nu = 107\,751.5$ cm^{-1} ($N = 64$), this peak is assigned as $[A^2\Pi_{u,3/2}]4d\pi_g$, $^1\Sigma_u^+$ with $v = 8$, $n^* = 3.67$. The β for channels $Cl^+(^3P_{0,1})$, $Cl^+(^3P_2)$, and $Cl^+(^1D_2)$ are 1.99, 0.07, and 1.22, and the branching ratios for them are 0.56, 0.94, and 1, respectively. In fact, this peak is assigned from the same vibrational progression as $N = 77$ discussed above. The β value for fragment $Cl^+(^3P_2)$ indicates that a large percent of it comes from the perpendicular transition to $[A^2\Pi_{u,3/2}]4d\sigma_g$, $^1\Pi_u$ that is neglected in the present discussion.

(iii) For $h\nu = 108\,425.9$ cm^{-1} ($N = 40$), this peak is assigned from two simultaneously excited Rydberg states: $[A^2\Pi_{u,3/2}]4d\pi_g$, $^1\Sigma_u^+$ with $v = 10$, $n^* = 3.66$ and $[A^2\Pi_{u,1/2}]6s\sigma_g$, $^1\Pi_u$ with $v = 5$, and $n^* = 3.98$. The β values for channels $Cl^+(^3P_j)$ and $Cl^+(^1D_2)$ are 1.24 and -0.25, respectively. The branching ratios for $Cl^+(^3P_{0,1})$, $Cl^+(^3P_2)$, and $Cl^+(^1D_2)$ are 0.53, 0.95, and 1, respectively. From the β values, it is known that the fragments $Cl^+(^1D_2)$ are mainly from the predissociation of $[A^2\Pi_{u,1/2}]6s\sigma_g$, $^1\Pi_u$, and a small part of them is from $[A^2\Pi_{u,3/2}]4d\pi_g$, $^1\Sigma_u^+$. The fragments $Cl^+(^3P_j)$ are mainly from the predissociation of $[A^2\Pi_{u,3/2}]4d\pi_g$, $^1\Sigma_u^+$. The channel for the production of $Cl^+(^3P_1)$ should be weak.

(iv) For $h\nu = 109\,101.0$ cm^{-1} ($N = 32$), this peak is assigned as $[A^2\Pi_{u,1/2}]6s\sigma_g$, $^1\Pi_u$ with $v = 7$, $n^* = 3.96$. The β for channels $Cl^+(^3P_j)$ and $Cl^+(^1D_2)$ are -0.90 and -0.82, respectively. The branching ratio for $Cl^+(^3P_j)$ and $Cl^+(^1D_2)$ are 0.72 and 1, respectively. From the β values, it is known that $[A^2\Pi_{u,1/2}]6s\sigma_g$, $^1\Pi_u$ should be the major excited Rydberg state. The intensities from the channel $Cl^+(^1D_2)$ are larger than those from $Cl^+(^3P_j)$ since the former correlates mainly with the singlet state excitations as discussed in Section III.B. It is also expected that the channel for $Cl^+(^3P_0)$ should have weaker intensities than the channels for $Cl^+(^3P_1)$ and $Cl^+(^3P_2)$.

It is noted that fragments $Cl^+(^1D_2)$ from the hot band excitation or from the vibrational excited Cl_2 have been observed in images $N = 64$ and 32 (see Figures 4 and 5). However, we have not obtained their branching ratios and β parameters due to the resolution of our instruments.

IV. Summary and Conclusion

The ion-pair dissociation dynamics of Cl_2 in the range 13.26−13.73 eV have been studied employing XUV laser and the velocity map imaging methods. The $Cl^-(^1S_0)$ ion-pair yield spectrum has been measured, and 80 velocity map imagings of $Cl^-(^1S_0)$ have been recorded for the strong bands in the spectrum. The experimental results are explained by the predissociation mechanism of Rydberg states. The ion-pair yield spectrum has been assigned based on the observed symmetry properties of Rydberg states. It is concluded that the couplings between the Rydberg states and ion-pair states are mainly due to the electrostatic interaction. The vibrational energy levels for the ion core $Cl_2^+(A^2\Pi_u)$ were derived by combining the previous results from the ZEKE spectrum[17] and the emission spectra[21] of $Cl_2^+(A^2\Pi_u) \rightarrow Cl_2^+(X^2\Pi_g)$.

The main experimental results are the following: (a) in the range 107 115−107 964 cm^{-1}, the major channels are the production of $Cl^+(^3P_j)$, and most of them are from parallel transitions with β values near +2, while the $Cl^+(^1D_2)$ channels have both positive and negative β values; and (b) in the range 107 964−110 740 cm^{-1}, the β values for the $Cl^+(^1D_2)$ channels are all negative, and most of the β values for the $Cl^+(^3P_j)$ channels are also negative; however, some of them are positive. In the range 109 100−110 740 cm^{-1}, the major channels are the production of $Cl^+(^1D_2)$.

Acknowledgment. This work is funded by Projects 20673066, 20773076, and 10734040 supported by the National Science Foundation of China, and Project 2007CB815200 supported by NKBRSF of China, the National High-Tech ICF Committee of China, and the Chinese Research Association of Atomic and Molecular Data.

References and Notes

(1) Peyerimhoff, S. D.; Buenker, R. *J. Chem. Phys.* **1981**, *57*, 279.
(2) Kokh, D. B.; Alekseyev, A. B.; Buenker, R. J. *J. Chem. Phys.* **2001**, *115*, 9298.
(3) Si, J.-H.; Ishiwata, T.; Obi, K. *J. Mol. Spectrosc.* **1991**, *147*, 334.
(4) Ishiwata, T.; Kasai, Y.; Obi, K. *J. Chem. Phys.* **1993**, *98*, 3620.
(5) Ishiwata, T.; Shinzawa, T.; Si, J.-H.; Obi, K.; Tanaka, T. *J. Mol. Spectrosc.* **1994**, *166*, 321.
(6) Ishiwata, T.; Kasai, Y.; Obi, K. *Chem. Phys. Lett.* **1996**, *261*, 175.
(7) Al-Kahali, M. S. N.; Donovan, R. J.; Lawley, K. P.; Min, Z.; Ridley, T. *J. Chem. Phys.* **1996**, *104*, 1825.
(8) Yamanouchi, K.; Tsuchizawa, T.; Miyawaki, J.; Tsuchiya, S. *Chem. Phys. Lett.* **1989**, *4*, 301.
(9) Nee, J. B. *J. Phys. B: At. Mol. Opt. Phys.* **1990**, *23*, 3325.
(10) Tsuchizawa, T.; Yamanouchi, K.; Tsuchiya, S. *J. Chem. Phys.* **1990**, *93*, 111.
(11) Berkowitz, J.; Mayhew, C. A.; Ruscic, B. *Chem. Phys.* **1988**, *123*, 317.
(12) Zhou, C.; Hao, Y.; Mo, Y. *J. Phys. Chem. A* **2008**, *112*, 8263.
(13) Hao, Y.; Zhou, C.; Mo, Y. *J. Phys. Chem. A.* **2005**, *109*, 5832.
(14) (a) Yang, J.; Hao, Y.; Li, J.; Zhou, C.; Mo, Y. *J. Chem. Phys.* **2005**, *122*, 134308 (b) *Ibid* **2007**, *127*, 209901.
(15) Hao, Y.; Zhou, C.; Mo, Y. *J. Phys. Chem. A* **2007**, *111*, 10887.
(16) Zhou, C.; Mo, Y. *J. Chem. Phys.* **2008**, *129*, 064312.
(17) Li, J.; Hao, Y.; Yang, J.; Zhou, C.; Mo, Y. *J. Chem. Phys.* **2007**, *127*, 104307.
(18) Eppink, A. T. J. B.; Parker, D. H. *Rev. Sci. Instrum.* **1997**, *68*, 3477.
(19) Stubbs, R. J.; York, T. A.; Comer, J. *J. Phys. B.* **1985**, *18*, 3229.
(20) Yencha, A. J.; Hopkirk, A.; Hiraya, A.; Donovan, R. J.; Goode, J. G.; Maier, R. R. J.; King, G. C.; Kvaran, A. *J. Phys. Chem.* **1995**, *99*, 7231.
(21) Tuckett, R. P.; Peyerimhoff, S. D. *Chem. Phys.* **1984**, *83*, 203.
(22) Huberman, F. P. *J. Mol. Spectrosc.* **1966**, *20*, 29.
(23) Al-Kahali, M. S. N.; Donovan, R. J.; Lawley, K. P.; Ridley, T. *J. Chem. Phys.* **1996**, *104*, 1833.
(24) Ridley, T.; Beattie, D.; Cockett, M. C. R.; Lawley, K. P.; Donovan, R. J. *Phys. Chem. Chem. Phys.* **2002**, *4*, 1398.
(25) Cantu, A. M.; Parkinson, W. H.; Grisendi, T.; Tagliaferri, G. *Phys. Scr.* **1985**, *31*, 579.
(26) Reinhold, E.; Ubachs, W. *Mol. Phys.* **2005**, *103*, 1329.
(27) Suit, A. G.; Hepburn, J. W. *Annu. Rev. Phys. Chem.* **2006**, *57*, 431.
(28) Lawley, K. P.; Flexen, A. C.; Maier, R. R. J.; Manck, A.; Ridley, T.; Donovan, R. J. *Phys. Chem. Chem. Phys.* **2002**, *4*, 1412.
(29) Zare, R. N.; Herschbach, R. D. *Proc. IEEE* **1963**, *51*, 173.
(30) Mo, Y.; Suzuki, T. *J. Chem. Phys.* **2000**, *112*, 3463.
(31) Lefebvre, H.; Field, R. W. *The Spectra and Dynamics of Diatomic Molecules*; Elsevier Academy Press: Amsterdam, 2004.
(32) . Werner, H. J.; Knowles, P. J.; Lindh, R.; Manby, F. R.; Schutz, M. MOLPRO, version 2006.1, a package of *ab initio* programs. See http://www.molpro.net.
(33) Wang, P.; Okuda, I. V.; Dimov, S. S.; Lipson, R. H. *J. Mol. Spectrosc.* **1998**, *190*, 213.

JP8097878